J. Fluid Mech. (1979), *vol.* 94, *part* 1, *pp.* 65–81
Printed in Great Britain

Sink flow in a rotating basin

By C. KRANENBURG
Department of Civil Engineering, Delft University of Technology, The Netherlands

(Received 30 August 1978 and in revised form 15 November 1978)

The flow of a homogeneous viscous liquid towards a sink in the interior of a rotating basin with a free surface, a horizontal bottom and a vertical side wall is considered. The conditions assumed are such that an Ekman layer occurs at the bottom beyond a small distance from the sink. A first-order correction to the Ekman model accounting for the influence of the inertial terms in the equations of motion is given for a special case. It is shown theoretically and experimentally that eccentric withdrawal from a circular basin causes a vortex at the sink and a counter-rotating gyre attached to the far wall.

1. Introduction

The research under discussion was done to make clear a certain aspect of the flow caused by the injection of compressed air at the bottom of a thermally stratified lake or reservoir. Air injection is sometimes used to increase the mixing between epilimnion and hypolimnion, thus destratifying the lake (Goossens & Van Pagee 1977; Kranenburg 1978). Local air injection induces a nearly horizontal sink flow in epilimnion and hypolimnion which is directed towards the injection point. The water transported through these layers enters a 'near field' surrounding the injection point, is mixed due to the turbulence caused by the air injection, and flows outwards horizontally as an interlayer of intermediate temperature and density. It has been found from destratification experiments in nature that the Coriolis force causes azimuthal velocities in epilimnion and hypolimnion which sometimes are larger by an order of magnitude than the radial components. A mathematical model of the destratification process in which viscous effects are ignored has been developed (Kranenburg 1978).

To obtain an understanding of the combined effects of viscosity and rotation, a simpler but related problem is examined in this paper, namely the local withdrawal from a single, homogeneous layer of viscous liquid in a rotating, shallow basin with a free surface, a horizontal bottom and a vertical side wall. The sink through which the liquid is withdrawn is remote from the side wall. It may be thought of as a vertical line sink extending from the free surface to the bottom, or a point sink at a certain depth. The influence of the actual shape or depth of the sink is likely to be confined to a relatively small region enclosing the sink. This point is discussed further in § 3.

The theory presented is connected with the studies by Barcilon (1967), Hide (1968) and Kuo & Veronis (1971). Both Barcilon and Hide consider the steady source–sink flow in a rotating, closed container in the absence of a free surface, the fluid being injected or withdrawn at the side walls. In the case of a constant-depth simply connected container, where the net mass flux at the side wall must be zero, the flow outside the viscous boundary layers at the end walls (the interior flow) is not influenced by the presence of the end walls. On the contrary, a net mass flux at a side wall in a multiply-

0022-1120/79/4276-7320 $02.00

connected container is entirely transported within the boundary layers at the side walls and end walls. This different behaviour is also discussed by Greenspan (1968). The influence of a free surface is examined by Kuo & Veronis. The flow is quasi-steady, the container is simply-connected, and again the sources and sinks are at the side wall. The presence of a free surface makes it possible to have a net mass flux also in the case of a simply-connected container. The boundary layers then play an essential role in the transport of mass, to a certain extent analogous to that in the case of a closed, multiply-connected container. A net inflow (or outflow) is found to cause a gyre in the interior of the flow, since the mass transport from the bottom boundary layer into the interior requires a rotational interior flow.

The case considered here differs in two major respects from that by Kuo & Veronis. Firstly, the sink is placed at some distance from the side wall, which in fact makes the container multiply-connected. As a result a vortex with its centre at the sink arises, which partly or completely (in an axisymmetric situation) annihilates the gyre found by Kuo & Veronis. Furthermore, the side-wall viscous boundary layers are of secondary importance, the mass transport towards the sink taking place within the bottom boundary layer and the interior. Secondly, the development of the flow from rest (relative to the rotating basin) is examined. It is found that initially the mass transport takes place for the larger part in the interior of the flow, but when a quasi-steady state has set in after a certain spin-up time all mass is transported within the bottom boundary layer. The analytic development is based on the Ekman model of rotating flow (§ 2). A first-order correction as regards the influence of the inertial terms in the equations of motion is given in § 3 for a special case. Some theoretical results are compared with laboratory experiments in § 4.

2. Ekman model

It is well known that, if certain conditions (to be specified later) are satisfied, an Ekman boundary layer will develop at the bottom of a rotating basin. Assuming a constant viscosity ν, or, in the case of turbulent flow, a constant eddy viscosity, the vertical velocity distribution in the Ekman layer is given by ($z = 0$ at the horizontal bottom)

$$u(x,y,z,t) = U(x,y,t)\,(1-e^{-kz}\cos kz) - V(x,y,t)\,e^{-kz}\sin kz \tag{2.1}$$

and

$$v(x,y,z,t) = U(x,y,t)\,e^{-kz}\sin kz + V(x,y,t)\,(1-e^{-kz}\cos kz), \tag{2.2}$$

where x, y are horizontal co-ordinates attached to the rotating basin, z is the vertical co-ordinate, u, v are horizontal velocity components, t is time, and $k = (f/2\nu)^{\frac{1}{2}}$. Here f is the Coriolis parameter ($= 2\Omega\sin\phi$, Ω is the angular velocity of the earth and ϕ the latitude). The velocity components U and V representing the flow in the region outside the Ekman layer (the interior flow region), do not depend on the vertical co-ordinate z. An estimate of the thickness δ of the Ekman layer is

$$\delta \sim (\nu/f)^{\frac{1}{2}}. \tag{2.3}$$

Equations (2.1) and (2.2) imply a horizontal transport of mass through the Ekman layer, which is normal to the velocity vector in the interior flow region (Ekman transport).

In terms of a horizontal length scale L^*, a velocity scale U^* and a time scale T^* the conditions for an Ekman layer to occur are

$$\frac{1}{fT^*} \ll 1, \quad Ro = \frac{U^*}{fL^*} \ll 1, \quad E = \frac{\nu}{f(L^*)^2} \ll 1, \tag{2.4}$$

where Ro is a Rossby number, and E an Ekman number. The first two conditions represent the requirement that the inertial terms in the equations of motions should be relatively small, the third condition indicates negligible shear stresses in lateral planes. We shall give appropriate expressions for the scales later.

The equation for the vorticity $\omega = \partial V/\partial x - \partial U/\partial y$ in the interior flow region is

$$\frac{\partial \omega}{\partial t} + U\frac{\partial \omega}{\partial x} + V\frac{\partial \omega}{\partial y} + (f+\omega)\left(\frac{\partial U}{\partial x} + \frac{\partial V}{\partial y}\right) = 0. \tag{2.5}$$

Assuming (2.4), the vorticity is small when compared with the Coriolis parameter, since

$$\frac{\omega}{f} \sim \frac{U^*}{fL^*} = Ro. \tag{2.6}$$

We may therefore approximate (2.5) in the first instance by

$$\frac{\partial \omega}{\partial t} + U\frac{\partial \omega}{\partial x} + V\frac{\partial \omega}{\partial y} + f\left(\frac{\partial U}{\partial x} + \frac{\partial V}{\partial y}\right) \simeq 0. \tag{2.7}$$

The continuity equation for a fluid element extending from the bottom to the free surface ($z = h$) is

$$\frac{\partial h}{\partial t} + \frac{\partial}{\partial x}\int_0^h u\,dz + \frac{\partial}{\partial y}\int_0^h v\,dz = 0. \tag{2.8}$$

The rigid-body rotation of the basin causes a paraboloidal free surface (in a uniform gravity field). We assume such small angular velocities of the basin that this deformation is negligible, which requires a Froude number, $(fL^*)^2/(gh)$, to be small compared to unity (Kuo & Veronis considered Froude numbers of order unity). The sink flow also causes a deformation of the free surface, in particular close to the sink. Restricting the analysis to relatively small discharges, so that the radius of the 'dimple' in the free surface remains small, this contribution to the deformation of the free surface may also be neglected for the larger part of the flow. Some further discussion of this point is given in § 5. Introducing the approximations $\partial h/\partial x \simeq \partial h/\partial y \simeq 0$, (2.8) becomes

$$-\frac{Q(t)}{A} + h\left(\frac{\partial U}{\partial x} + \frac{\partial V}{\partial y}\right) \simeq \frac{\omega}{2k}, \tag{2.9}$$

where Q is the discharge withdrawn, and A the surface area of the basin. The right-hand side of (2.9) represents the so-called Ekman suction (or injection), a vertical transport of mass from the interior flow into the Ekman layer (or conversely) (e.g. Greenspan 1968). Eliminating the divergence $\partial U/\partial x + \partial V/\partial y$ of the interior flow field from (2.7) and (2.8) yields as an equation for the vorticity

$$\frac{D\omega}{Dt} + \frac{f}{h}\left(\frac{Q}{A} + \frac{\omega}{2k}\right) = 0, \tag{2.10}$$

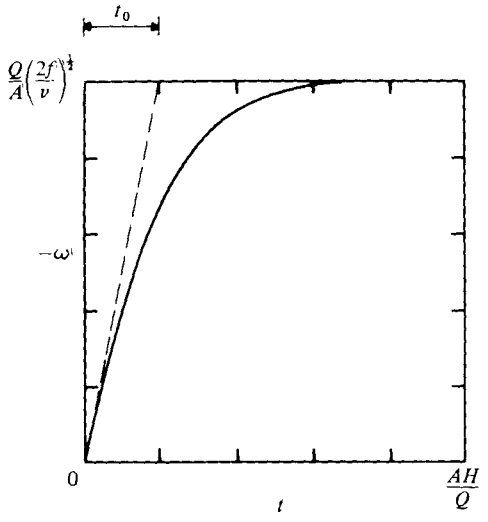

FIGURE 1. Time evolution of vorticity. $\alpha = 0{\cdot}2$.

where $D/Dt = \partial/\partial t + U\partial/\partial x + V\partial/\partial y$ is the material derivative. The water depth h follows from

$$\frac{dh}{dt} + \frac{Q}{A} = 0, \quad h(0) = H, \tag{2.11}$$

where H is the initial water depth (Q is assumed to be zero when $t \leqslant 0$).

Integrating (2.11) and (2.10) yields the vorticity of a particular fluid element in the interior flow region as a function of time. However, (2.10) holds for all fluid elements in the interior flow region. Consequently, these elements all attain the same vorticity at a certain instant, and the voriticity does not change in horizontal directions ($\partial\omega/\partial x = \partial\omega/\partial y = 0$). Therefore (2.10) is not only valid for a single element but also for the interior flow region as a whole. Since the fluid is at rest at $t = 0$, the initial condition for the vorticity equation (2.10) is $\omega(0) = 0$. The different behaviour of fluid entering the interior flow region as a consequence of upwelling at the side wall is discussed later.

The solution of (2.10) in the case of a constant discharge Q ($t > 0$) is, see figure 1,

$$\omega = -\frac{Q}{A}\left(\frac{2f}{\nu}\right)^{\frac{1}{2}}\left[1 - \left(\frac{h}{H}\right)^{1/\alpha}\right], \tag{2.12}$$

where

$$\alpha = \frac{Q}{A}\left(\frac{2}{f\nu}\right)^{\frac{1}{2}}. \tag{2.13}$$

Since $\omega \sim U^*/L^*$, and the spin-up time $t_0 \sim H/(\nu f)^{\frac{1}{2}}$ (figure 1), an obvious choice for the scale quantities involved is

$$\frac{U^*}{L^*} = \frac{Q}{A}\left(\frac{f}{\nu}\right)^{\frac{1}{2}} \quad \text{and} \quad T^* = \frac{H}{(\nu f)^{\frac{1}{2}}}.$$

The length scale L^* is associated with the size of the basin. We therefore assume $L^* = A^{\frac{1}{2}}$. The conditions (2.4) then become, respectively,

$$\delta/H \ll 1, \quad \alpha \ll 1, \quad \delta^2/A \ll 1. \tag{2.14}$$

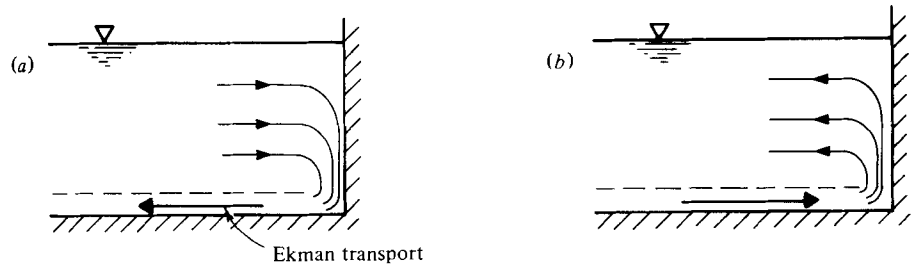

FIGURE 2. Flow at side wall. (*a*) Downwelling, (*b*) upwelling.

The first condition indicates that the Ekman layer thickness should be small when compared with the water depth; the second that the time [$\sim H/(\nu f)^{\frac{1}{2}}$] to reach the final vorticity should be much less than the time ($= AH/Q$) needed to empty the basin. The third condition is less restrictive than the first, since in general $A > H^2$.

2.1. *Boundary condition at the side wall*

In the case under consideration the boundary layer at the side wall is not essential for the mass transport (also see § 2.2), but only serves to reduce the velocity at the side wall to zero. Therefore, the only boundary condition at the side wall we consider is a zero net flux normal to it, that is

$$\int_0^h \mathbf{u}.\mathbf{n}\,dz = 0, \tag{2.15}$$

where $\mathbf{u}$ is the (horizontal) velocity vector ($\mathbf{u} = (u, v)$), and $\mathbf{n}$ is the unit vector normal to the side wall. Substituting from (2.1) and (2.2), equation (2.15) gives

$$\mathbf{U}.\mathbf{n} \simeq \frac{1}{2kh}\mathbf{U}.\mathbf{s}, \tag{2.16}$$

where $\mathbf{U}$ is the (horizontal) velocity vector of the interior flow, and $\mathbf{s}$ is the unit vector tangential to the side wall. The physical interpretation of (2.16) is that the Ekman transport at the side wall is compensated by an interior flow normal to the wall and downwelling (Ekman transport inwards, figure 2*a*) or upwelling (Ekman transport outwards, figure 2*b*) at the side wall. It follows from (2.14) and (2.16) that

$$|\mathbf{U}.\mathbf{n}| \ll |\mathbf{U}.\mathbf{s}|.$$

Equation (2.16) can be utilized to obtain an expression for the circulation $\oint \mathbf{U}.d\mathbf{s}$ along the side wall. The equations of motion for the interior flow may be written (a possible centrifugal force is absorbed in the pressure term, and $-\omega \ll f$)

$$\frac{\partial \mathbf{U}}{\partial t} + \nabla\left[\tfrac{1}{2}(\mathbf{U}.\mathbf{U}) + \frac{p}{\rho}\right] + \mathbf{f}\times\mathbf{U} \simeq 0,$$

where $\mathbf{f} = (0, 0, f)$. Forming the scalar product of this equation with a vector element $d\mathbf{s}$ along the side wall and integrating yields for the circulation along the wall

$$\frac{d}{dt}\oint \mathbf{U}.d\mathbf{s} + \oint d\mathbf{s}.\nabla\left[\tfrac{1}{2}(\mathbf{U}.\mathbf{U}) + \frac{p}{\rho}\right] + \oint d\mathbf{s}.(\mathbf{f}\times\mathbf{U}) = 0;$$

U and p are single-valued functions; the second term therefore vanishes. The third term may be written

$$\oint d\mathbf{s}.(\mathbf{f}\times\mathbf{U}) = f\oint \frac{\mathbf{U}.\mathbf{n}}{\mathbf{U}.\mathbf{s}}\,\mathbf{U}.d\mathbf{s}.$$

This result and the boundary condition (2.16) then change the above equation to

$$\frac{d}{dt}\oint \mathbf{U}.d\mathbf{s} + \frac{1}{h}\left(\frac{\nu f}{2}\right)^{\frac{1}{2}}\oint \mathbf{U}.d\mathbf{s} = 0.$$

The solution of this equation is

$$\oint \mathbf{U}.d\mathbf{s} = C\exp\left[-\left(\frac{\nu f}{2}\right)^{\frac{1}{2}}\int_0^t \frac{dt_1}{h(t_1)}\right].$$

The constant of integration C is equal to zero, the fluid being at rest at $t = 0$. The negative argument of the exponential function indicates that the solution of a vanishing circulation along the side wall is stable. We thus obtain for all t

$$\oint \mathbf{U}.d\mathbf{s} = 0. \tag{2.17}$$

This result shows that, if **U** does not vanish everywhere at the wall, there must be at least two stagnation points at the wall. We shall see later that these two stagnation points are related to the occurrence of a vortex near the sink and a counterrotating gyre attached to the far wall.

2.2. *Interior flow field*

The definition of the vorticity and the continuity equation (2.9) yield the equations for the interior flow,

$$\frac{\partial V}{\partial x} - \frac{\partial U}{\partial y} = \omega \tag{2.18}$$

and

$$\frac{\partial U}{\partial x} + \frac{\partial V}{\partial y} = \frac{1}{h}\left(\frac{\omega}{2k} + \frac{Q}{A}\right). \tag{2.19}$$

The vorticity of the interior flow follows from (2.10). It depends on time, but not on the horizontal co-ordinates. The vorticity of the fluid entering the interior flow region at the side wall (upwelling of fluid transported outwards in the Ekman layer) is different. The order of magnitude of the inward velocity $\mathbf{U}.\mathbf{n}$ of this fluid is, see (2.16),

$$\mathbf{U}.\mathbf{n} \sim \frac{1}{2kh}U^* \sim \frac{Q}{HA^{\frac{1}{2}}}.$$

The time this fluid needs to adapt its vorticity to that of the interior flow is of order T^*. The distance the fluid element travels in the direction normal to the wall within this time interval is

$$(\mathbf{U}.\mathbf{n})T^* \sim \alpha A^{\frac{1}{2}}.$$

Since α is assumed small, there is only a relatively thin layer at the wall where the vorticity differs from that in the remaining part of the interior flow region.

Neglecting this effect, the right-hand sides of (2.18) and (2.19) become functions of

time only. We may then introduce a stream function Ψ and potential functions Φ_1 and Φ_2 not depending on time, according to

$$U = -\omega A \frac{\partial \Psi}{\partial y} + \frac{1}{h}\left(\frac{\omega}{2k} A + Q\right) \frac{\partial \Phi_1}{\partial x} + \frac{\omega}{2kh} A \frac{\partial \Phi_2}{\partial x} \tag{2.20}$$

and

$$V = \omega A \frac{\partial \Psi}{\partial x} + \frac{1}{h}\left(\frac{\omega}{2k} A + Q\right) \frac{\partial \Phi_1}{\partial y} + \frac{\omega}{2kh} A \frac{\partial \Phi_2}{\partial y}. \tag{2.21}$$

On substitution of (2.20) and (2.21) into (2.18) and (2.19), Ψ, Φ_1 and Φ_2 are found to satisfy the equations

$$\frac{\partial^2 \Psi}{\partial x^2} + \frac{\partial^2 \Psi}{\partial y^2} = \frac{1}{A}, \tag{2.22}$$

$$\frac{\partial^2 \Phi_1}{\partial x^2} + \frac{\partial^2 \Phi_1}{\partial y^2} = \frac{1}{A} \tag{2.23}$$

and

$$\frac{\partial^2 \Phi_2}{\partial x^2} + \frac{\partial^2 \Phi_2}{\partial y^2} = 0. \tag{2.24}$$

The boundary conditions follow from (2.16). Since the coefficient $1/2kh$ in this equation is much less than unity, it suffices to take into account on the right-hand side of (2.16) only the leading terms of (2.20) and (2.21). We then obtain

$$-\omega A \frac{\partial \Psi}{\partial s} + \frac{1}{h}\left(\frac{\omega}{2k} A + Q\right) \frac{\partial \Phi_1}{\partial n} + \frac{\omega}{2kh} A \frac{\partial \Phi_2}{\partial n} \simeq \frac{\omega}{2kh} A \frac{\partial \Psi}{\partial n}, \tag{2.25}$$

where s and n are co-ordinates along and normal to the wall. In order that stream function and potential functions do not depend on time, the following conditions at the side wall must be satisfied:

$$\frac{\partial \Psi}{\partial s} = 0, \quad \frac{\partial \Phi_1}{\partial n} = 0 \quad \text{and} \quad \frac{\partial \Phi_2}{\partial n} = \frac{\partial \Psi}{\partial n}. \tag{2.26)–(2.28}$$

The above equations reveal the physical significance of Ψ, Φ_1 and Φ_2. Initially ($t \ll T^*$) the vorticity ω is still small, and the velocities follow from the potential function Φ_1. The flow is then almost identical to that in a non-rotating reservoir, the transport of fluid towards the sink taking place over the whole depth (figure 3*a*). When time elapses, the vorticity increases, so that the factors multiplying derivatives of Ψ and Φ_2 in (2.20) and (2.21) increase. When ω has reached its final value $-2kQ/A$ [see (2.12)] the influence of the potential function Φ_1 vanishes. The right-hand side of the continuity equation (2.9) shows that, as ω increases, the Ekman layer suction increases. The (vertical) suction velocity $\omega/2k$ tends to the vertical velocity of the free surface ($-Q/A$) as ω tends to its final value. Consequently, the transport of fluid towards the sink then takes place completely within the Ekman layer, whereas the streamlines of the interior flow are closed (figure 3*b*). This result for (quasi-)steady flow is well known.

The net flux at the side wall due to Φ_2 vanishes [this follows from (2.28) and (2.17)]. As discussed in the introduction, the flow resulting from this contribution therefore takes place in the interior and additional transport within the side-wall boundary layer is absent.

The functions Φ_1 and Ψ are singular at the sink. Introducing cylindrical co-ordinates

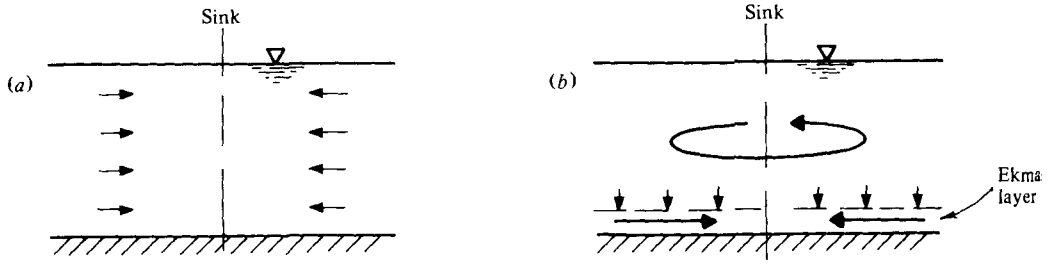

FIGURE 3. Principles of flow field. (*a*) Initial phase, (*b*) final phase.

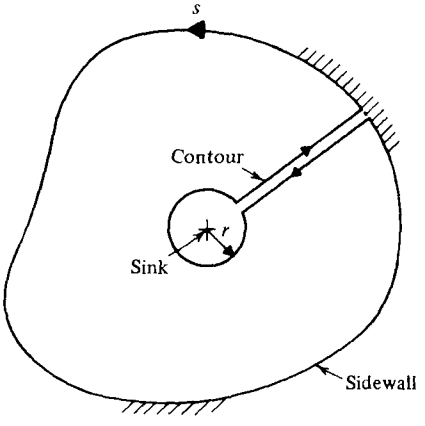

FIGURE 4. Application of Stokes's theorem.

(with the vertical axis at the sink and radius r), the continuity equation when applied to the interior flow region yields, for $r \to 0$,

$$2\pi rhH = -\left(Q + \frac{\omega}{2k}A\right). \tag{2.29}$$

Here U now is the radial velocity component. The last term in (2.29) represents the transport through the Ekman layer. It follows from (2.29) that

$$\Phi_1 \to -\frac{1}{2\pi}\ln\frac{r}{r_0} \quad \text{if} \quad r \to 0, \tag{2.30}$$

where r_0 is an arbitrary constant.

The singularity in the stream function Ψ can be found by applying Stokes' theorem to the region enclosed by the contour shown in figure 4. This gives

$$\oint \mathbf{U}.d\mathbf{s} - (2\pi r V)_{r\to 0} = \omega A.$$

Here V now is the azimuthal velocity component. Using (2.17) we obtain†

$$V \to -\omega A/2\pi r \quad \text{and} \quad \Psi \to -\frac{1}{2\pi}\ln\left(\frac{r}{r_0}\right) \quad \text{if} \quad r \to 0. \tag{2.31}$$

The singularity in Ψ will not occur if the sink is situated at the side wall. This case was treated by Kuo & Veronis (1971).

† This result can also be derived by using the Ekman-transport concept.

Equations (2.29) and (2.30) show that the azimuthal velocity V in the final phase is an order of magnitude (namely by a factor $h/2k$) larger than the radial velocity U in the initial phase.

All equations and boundary conditions determining the functions Ψ, Φ_1 and Φ_2 are time-independent. This therefore also holds for the functions themselves.

3. First-order correction to Ekman model for a special case

The boundary layer within a certain distance from the sink is not of the Ekman type, since the relative magnitude of the inertial terms in the equations of motion increases, and becomes large, as the distance from the sink decreases. To examine the boundary-layer flow closer to the sink in somewhat greater detail, we consider in this section the final (quasi-steady) phase of centric withdrawal from a circular basin. This case represents the simplest flow configuration that exhibits the singular behaviour at the sink. Extension to the more general situation discussed in § 2 is straightforward.

In all cases where the sink is not at the bottom, the boundary layer breaks up under the sink to establish an upward, rotating flow along the vertical axis; this flow resembles that occurring in the core of a tornado (cf. Turner 1966, Burggraf & Foster 1977, for instance). Lewellen (1962) gives a formal series expansion of the governing equations in a small parameter, which in the present notation may be written $[Q/(\Gamma^0 L)]^2$. Here Γ^0 is the scale of the circulation and L a local horizontal length scale. Lewellen shows that the leading terms in the expansions for the circulation, and radial and vertical velocity components do not depend on the vertical co-ordinate. This indicates that the interior flow in the problem under discussion becomes appreciably disturbed by the shape or depth of the sink at horizontal distances L of order Q/Γ^0. Substituting from equation (3.5) given below would yield $L \sim (\nu/f)^{\frac{1}{2}}$, which is much less than the total depth, see (2.3) and (2.14). This conclusion is in qualitative agreement with the experiments described in § 4. In the analysis which follows we restrict ourselves to the region where the bottom boundary layer still exists.

The boundary-layer equations are, in cylindrical co-ordinates,

$$u\frac{\partial u}{\partial r}+w\frac{\partial u}{\partial z}-\frac{v^2}{r}-fv=-\frac{V^2}{r}-fV+\nu\frac{\partial^2 u}{\partial z^2}; \tag{3.1}$$

$$u\frac{\partial v}{\partial r}+w\frac{\partial v}{\partial z}+\frac{uv}{r}+fu=\nu\frac{\partial^2 v}{\partial z^2}; \tag{3.2}$$

and

$$\frac{\partial}{\partial r}ru+r\frac{\partial w}{\partial z}=0. \tag{3.3}$$

Here u, v and w are the radial, azimuthal and vertical velocity components. V is the azimuthal velocity of the interior flow. These equations are identical to the equations given by Burggraf, Stewartson & Belcher (1971), except for the Coriolis terms. These authors examined the boundary layer at the bottom of a non-rotating container induced by a potential vortex. Some of their results for small radius apply to the present case, since the Coriolis terms are then of secondary importance. Burggraf *et al.* obtained the following results of interest here for r tending to zero. The boundary layer attains a 'double structure' comprising an inner and an outer boundary layer. The inner layer

develops at the bottom. Its thickness is of order $r(\nu/\Gamma^0)^{\frac{1}{2}}$. The inner layer has a similarity structure, the similarity variable being $z/r(\nu/\Gamma^0)^{\frac{1}{2}}$, which structure is determined by the local properties of the flow. The (absolute value of the) radial velocity component in this layer is an order of magnitude larger than the azimuthal component. In the outer layer the horizontal velocity vector rotates from the negative radial direction in the inner layer to the azimuthal direction of the undisturbed flow, but the magnitude of the velocity is independent of z. The outer structure depends on the history of the boundary layer. Since $u < 0$, the boundary conditions at the side wall of the container therefore act upon the outer structure. All velocity components in the outer layer are inversely proportional to the radius $r(r \to 0)$, which implies a finite volume flux towards the axis. It is this result that makes the analysis of Burggraf *et al.* applicable to the problem under consideration.

Introducing, for the present problem, a vertical length scale δ^0, a radial length scale L^0, a horizontal velocity scale $U^0 = \Gamma^0/L^0$, and a vertical velocity scale $W^0 = U^0\delta^0/L^0$, the behaviour of the boundary layer for $r \to 0$ indicates that the scales may be so chosen that

$$-2\pi r \int_0^\infty u\,dz = Q \sim L^0 U^0 \delta^0 = \Gamma^0 \delta^0. \tag{3.4}$$

Non-dimensionalizing the boundary-layer equations and requiring that all coefficients be unity to preserve the validity of the equations for all r, yields for the scale quantities

$$\delta^0 = (\nu/f), \quad L^0 = [Q/(\nu f)^{\frac{1}{2}}]^{\frac{1}{2}}, \quad \Gamma^0 = Q(f/\nu)^{\frac{1}{2}} \quad \text{and} \quad W^0 = (\nu f)^{\frac{1}{2}}. \tag{3.5}$$

Apparently, the vertical length scale and the scale of the circulation are the same for $r \to 0$ as those for the Ekman model. The radial length scale is different, since L^0 is of order $R\alpha^{\frac{1}{2}}$ and L^* is of order R, where R is the radius of the basin.† These results imply that the (outer) boundary-layer thickness and the circulation are smooth functions of the radius as r goes to zero. It would be interesting to have numerical solutions of the boundary-layer equations to verify these conclusions. A similar problem, namely the boundary-layer flow induced by a potential vortex in a rotating container, was suggested by Brown & Stewartson (1976) in a somewhat different context. The flow will be of the boundary-layer type, provided $(\delta^0/L^0)^2 = \nu/\Gamma^0 \ll 1$.

3.1. *Expansion for small* α

The above discussion will serve to yield a matching condition for a first-order correction to the Ekman model. As regards an expansion about the Ekman model the vertical length scale, radial length scale, horizontal velocity scale and vertical velocity scale may be conveniently chosen as, respectively,

$$\left(\frac{2\nu}{f}\right)^{\frac{1}{2}}, \quad R, \quad \frac{2^{\frac{1}{2}}}{\pi}\frac{\Gamma^0}{R} \quad \text{and} \quad \frac{2}{\pi}\frac{\Gamma^0}{R^2}\left(\frac{\nu}{f}\right)^{\frac{1}{2}},$$

† L^0 measures the size of the region surrounding the sink where the inertial terms dominate the Coriolis terms.

where Γ^0 is given by (3.5). Normalizing the boundary-layer equations with these scale quantities yields the dimensionless equations

$$\alpha\left(u\frac{\partial u}{\partial r}+w\frac{\partial u}{\partial z}-\frac{v^2}{r}+\frac{V^2}{r}\right)=v-V+\frac{1}{2}\frac{\partial^2 u}{\partial z^2}, \tag{3.6}$$

$$\alpha\left(u\frac{\partial v}{\partial r}+w\frac{\partial v}{\partial z}+\frac{uv}{r}\right)=-u+\frac{1}{2}\frac{\partial^2 v}{\partial z^2} \tag{3.7}$$

and

$$\frac{\partial}{\partial r}ru+r\frac{\partial w}{\partial z}=0. \tag{3.8}$$

One set of boundary conditions derives from the no-slip condition at the bottom $z=0$. For the present, the horizontal interior velocity components ($U=0$, $V\neq 0$) are prescribed to yield a second set of boundary conditions, and the aim is to find the vertical interior velocity component (the suction velocity). In a second step we equate the suction velocity to the vertical velocity of the free surface in order to determine the final azimuthal velocity distribution.

In the first instance we assume a regular asymptotic expansion in powers of the Rossby number α,

$$(u,v,w)=(u_0,v_0,w_0)+\alpha(u_1,v_1,w_1)+\ldots, \tag{3.9}$$

where the functions u_j, v_j and w_j ($j=0,1,\ldots$) are assumed to be of order unity. The zero-order equations are

$$\frac{1}{2}\frac{\partial^2 u_0}{\partial z^2}+v_0=V,\quad \frac{1}{2}\frac{\partial^2 v_0}{\partial z^2}-u_0=0,\quad \frac{\partial}{\partial r}ru_0+r\frac{\partial w_0}{\partial z}=0. \tag{3.10}$$

These equations yield, together with the boundary conditions, the Ekman-layer solution

$$u_0=-V\lambda,\quad v_0=V(1-\mu),\quad w_0=\frac{1}{2r}\frac{d}{dr}(rV)(1-\lambda-\mu),$$

where $\lambda=\exp(-z)\sin z$, and $\mu=\exp(-z)\cos z$. The first-order equations are

$$\frac{1}{2}\frac{\partial^2 u_1}{\partial z^2}+v_1=F_{u0}, \tag{3.11}$$

$$\frac{1}{2}\frac{\partial^2 v_1}{\partial z^2}-u_1=F_{v0} \tag{3.12}$$

and

$$\frac{\partial}{\partial r}ru_1+r\frac{\partial w_1}{\partial z}=0, \tag{3.13}$$

where F_{u0} and F_{v0} are known functions of r and z;

$$F_{u0}=VV'\lambda^2-\frac{V}{2r}\frac{d}{dr}(rV)(1-\lambda-\mu)\lambda'-\frac{V^2}{r}(1-\mu)^2+\frac{V^2}{r}$$

and

$$F_{v0}=-VV'\lambda(1-\mu)-\frac{V}{2r}\frac{d}{dr}(rV)(1-\lambda-\mu)\mu'-\frac{V^2}{r}\lambda(1-\mu),$$

where $V'=dV/dr$, $\lambda'=d\lambda/dz$ and $\mu'=d\mu/dz$. Introducing the complex variables $u_{c1}=u_1+iv_1$ and $F_{c0}=F_{u0}+iF_{v0}$, (3.11) and (3.12) may be written as

$$\frac{1}{2}\frac{\partial^2 u_{c1}}{\partial z^2}-iu_{c1}=F_{c0}.$$

The boundary conditions are $u_{c1}(r, 0) = u_{c1}(r, \infty) = 0$. On integration with respect to z this equation yields

$$u_{c1} = \frac{1}{\beta}\left[e^{-\beta z}\int_0^\infty F_{c0}\, e^{-\beta z}\, dz - e^{\beta z}\int_z^\infty F_{c0}\, e^{-\beta z_1}\, dz_1 - e^{-\beta z}\int_0^z F_{c0}\, e^{\beta z_1}\, dz_1\right], \tag{3.14}$$

where $\beta = 1 + i$. At this stage a physically unrealistic singularity at the axis comes out. The function F_{c0} and therefore the complex velocity u_{c1} are proportional to r^{-3} as $r \to 0$. This situation becomes increasingly worse in higher-order approximations. This behaviour for $r \to 0$ contradicts the conclusions drawn earlier in this section. Obviously, this anomaly is caused by the asymptotic expansion (3.9). Several methods exist to remove a singularity which emerges in an asymptotic expansion, but which does not occur in the original equations. We shall use a 'renormalization technique' in the sense that the singularity is removed after the expansion has been performed (e.g. Nayfeh 1973).

Equations (3.13) and (3.14) yield for the first-order vertical velocity in the interior flow region

$$w_1(r, \infty) = \frac{1}{r}\frac{d}{dr}\left[c_1 r V V' + c_2 V \frac{d}{dr}(rV) + c_3 V^2\right], \tag{3.15}$$

where

$$c_1 = \int_0^\infty \lambda[\lambda^2 - (1-\mu)^2]\, dz = -\tfrac{17}{60}, \tag{3.16a}$$

$$c_2 = -\frac{1}{2}\int_0^\infty (1-\lambda-\mu)\,[\lambda\lambda' + (1-\mu)\,\mu']\, dz = \tfrac{1}{4} + \tfrac{1}{2}c_1 = \tfrac{13}{120} \tag{3.16b}$$

and

$$c_3 = \int_0^\infty \lambda[1 - 2(1-\mu)^2]\, dz = -\tfrac{2}{15}. \tag{3.16c}$$

The relation between c_2 and c_1 follows from integration of (3.16b) by parts.

We now equate the vertical interior velocity (with error of order α^2) to the vertical velocity of the free surface, which is, in dimensionless form, equal to $-\frac{1}{2}$. This gives

$$\frac{1}{2r}\frac{d}{dr}(rV) + \frac{\alpha}{r}\frac{d}{dr}[(c_1+c_2)\, rVV' + (c_2+c_3)\, V^2] \simeq -\tfrac{1}{2}.$$

This equation may be integrated once to give ($V(1) = 0$)

$$\Gamma + \frac{2\alpha}{r^2}[(c_1+c_2)\, r\Gamma\Gamma' + (c_3-c_1)\,\Gamma^2] = \tfrac{1}{2}(1-r^2), \tag{3.17}$$

where $\Gamma = rV$. According to the discussion of the solution for $r \to 0$, Γ should remain finite as r tends to zero. Adopting Lighthill's method to remove the singularity in Γ (e.g. Nayfeh 1973), we assume the expansions

$$\Gamma = \Gamma_0(s) + \alpha\Gamma_1(s) + \ldots$$

and

$$r^2 = s + \alpha\xi_1(s) + \ldots.$$

On substitution into (3.17) this yields as a zero-order solution the trivial result

$$\Gamma_0 = \tfrac{1}{2}(1-s) \tag{3.18}$$

and as a first-order solution

$$\Gamma_1 = -4(c_1+c_2)\,\Gamma_0\frac{d\Gamma_0}{ds} - 2(c_3-c_1)\frac{\Gamma_0^2}{s} - \tfrac{1}{2}\xi_1.$$

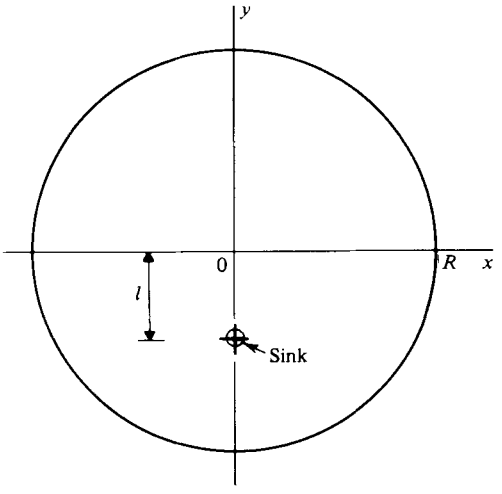

FIGURE 5. Definition sketch of circular basin.

The singularity in Γ_1 can be removed by letting

$$\xi_1 = -4(c_3 - c_1)\frac{\Gamma_0^2}{s}$$

so that
$$\Gamma = [\tfrac{1}{2} + \alpha(c_1 + c_2)](1-s) + O(\alpha^2) \tag{3.19}$$

and
$$r^2 = s - \alpha(c_3 - c_1)\frac{(1-s)^2}{s} + O(\alpha^2). \tag{3.20}$$

This solution implies that Γ is a smooth function for all radii. Thus the physically unrealistic singular perturbations, which (3.17) in principle permits since the expansion parameter multiplies the highest derivative, are suppressed. It is well known that the absence of singular perturbations is a condition for Lighthill's method to yield realistic results.

The solution obtained is not valid in a certain region ($r \sim R\alpha^{\frac{1}{2}}$) near the sink. That it nevertheless can be valid at larger distances is related to the parabolic character of the boundary-layer equations (3.1) through (3.3), which precludes upstream influence.

4. Theoretical and experimental results for a circular basin

The interior flow pattern as predicted by the Ekman model (§ 2) is determined by the functions Ψ, Φ_1 and Φ_2. Here we devote attention to the stream function Ψ only, since this function represents the influence of the rotation on the interior flow. It also determines to a large extent the flow in the final quasi-steady phase in the case where Q is constant. The potential function Φ_1 represents the flow pattern in the absence of rotation, and is of less interest here. The contribution of the potential function Φ_2 is of secondary importance, because of the small factor $1/2kh$ in (2.20) and (2.21).

The solution of (2.22) for a circular basin (figure 5), which satisfies the boundary

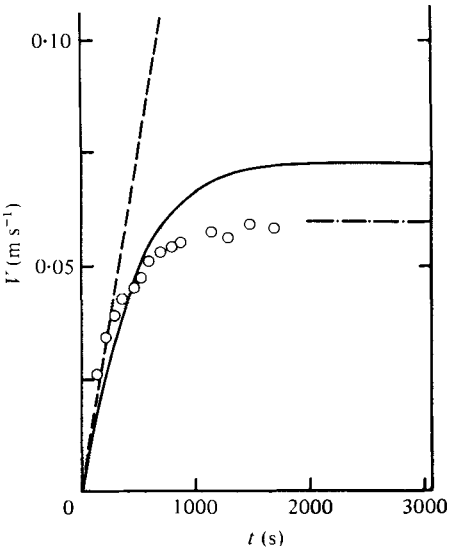

FIGURE 6. Time evolution of azimuthal velocity. – – –, inviscid solution; ——, zero-order (Ekman) solution; –·–, first-order solution; ○, experiment. $r = 0{\cdot}097$ m, $f = 2\Omega = 0{\cdot}161\ \mathrm{s}^{-1}$, $Q = 0{\cdot}0792 \times 10^{-3}\ \mathrm{m}^3\ \mathrm{s}^{-1}$, $\alpha = 0{\cdot}158$.

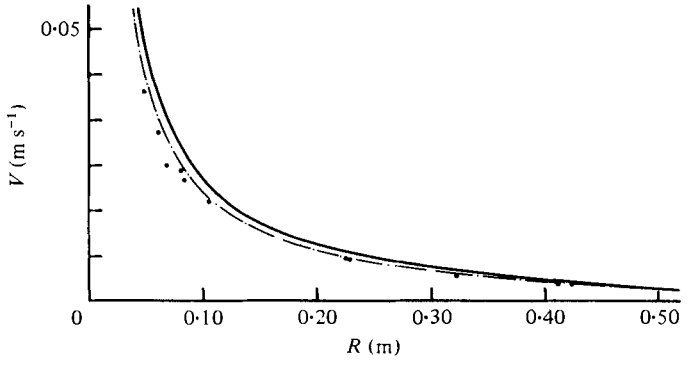

FIGURE 7. Radial distribution of final azimuthal velocity. ——, zero-order (Ekman) solution; –·–, first-order solution; ●, experiment. $f = 2\Omega = 0{\cdot}091\ \mathrm{s}^{-1}$, $Q = 0{\cdot}0410 \times 10^{-3}\ \mathrm{m}^3\ \mathrm{s}^{-1}$, $\alpha = 0{\cdot}109$.

condition (2.26) and has the correct singular behaviour at the sink according (2.31), is

$$\Psi = \frac{1}{4\pi} \ln \left[\frac{l^2}{R^2} \frac{x^2 + (y + R^2/l)^2}{x^2 + (y+l)^2} \right] + \frac{1}{4\pi} \frac{x^2 + y^2}{R^2}. \tag{4.1}$$

The co-ordinates of the sink are $x = 0$, $y = -l$.

In the case of centric withdrawal the solution simplifies to that given by (3.18). The corresponding final radial and azimuthal velocities become

$$U = 0, \quad V = \left(\frac{2f}{\nu}\right)^{\frac{1}{2}} \frac{Q}{2\pi r} \left(1 - \frac{r^2}{R^2}\right). \tag{4.2}$$

This result may be derived more simply directly. Figure 6 shows the azimuthal velocity V at a fixed radius as a function of time. It is seen that the viscous and inviscid (slip conditions at the bottom) solutions initially coincide, but that the viscous

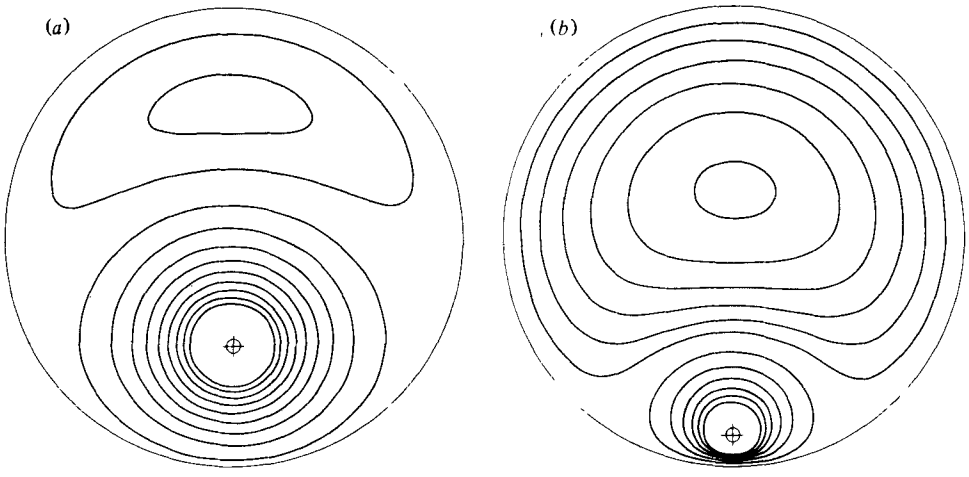

FIGURE 8. Theoretical streamlines Ψ = constant. (*a*) $l/R = 0{\cdot}467$; (*b*) $l/R = 0{\cdot}867$.

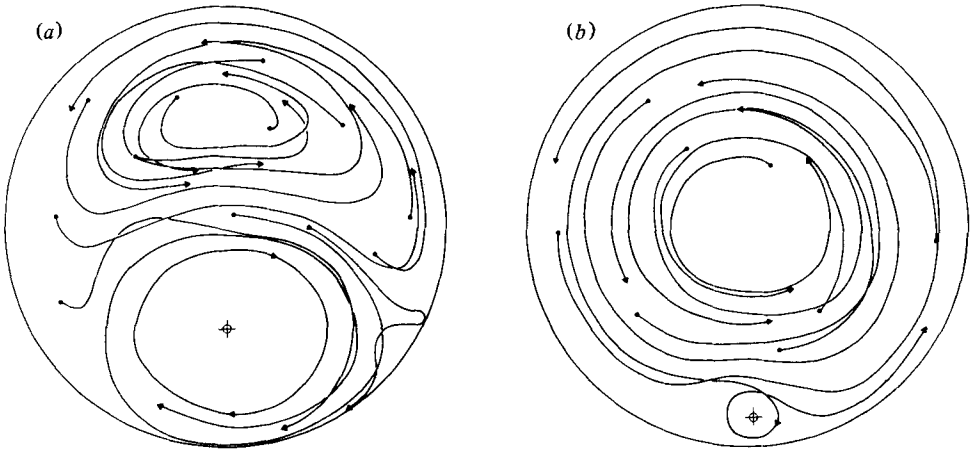

FIGURE 9. Experimental path lines of interior flow in final phase. $f = 2\Omega = 0{\cdot}29\ \mathrm{s}^{-1}$, $Q = 0{\cdot}041 \times 10^{-3}\ \mathrm{m}^3\ \mathrm{s}^{-1}$, $\alpha = 0{\cdot}061$. (*a*) $l/R = 0{\cdot}467$; (*b*) $l/R = 0{\cdot}867$.

solution branches off to a constant final value. Figure 7 shows the radial distribution of the final azimuthal velocities.

Figure 8 shows theoretical streamlines Ψ = constant for two eccentricities l/R. It is seen that a vortex develops near the sink, much as in the case of centric withdrawal, and that a counterrotating gyre is generated at the far wall. The stagnation points at the side wall separate regions with upwelling and downwelling [cf. equation (2.28)], upwelling occurring at the far wall.

Experiments were done in a circular tank, diameter 1·50 m and maximum water depth 0·20 m, placed on a turntable rotating in clockwise direction. The angular velocities of the turntable (0·04–0·14 rad/s) were so low that the deformation of the free surface owing to the centrifugal force was negligibly small. In the experiments with centric withdrawal water was withdrawn through a small pipe at some distance above the bottom. The Ekman layer was visualized with potassium permanganate crystals

sprinkled on the bottom. Except very close to the sink, the angle between streaklines and azimuthal direction was nearly 45 degrees, which is in agreement with the theory of the Ekman layer. Near the sink the flow at the bottom was radially directed, in accord with the discussion in § 3. Azimuthal velocities of the interior flow were determined with a micropropeller (figure 6) and by measuring the travelling times of a float at the free surface (figure 7). The accuracy of the micro-propeller measurements is about ± 10 per cent for the lowest velocities and about ± 5 per cent for the largest velocities shown in figure 6. In the case of the float the accuracies are about ± 1 and ± 3 per cent, respectively.

Figures 6 and 7 show that the theory predicts the velocity distribution correctly. The first-order correction appears to account for the greater part of the discrepancy between zero-order (Ekman) solution and observed velocities.

In the experiments with eccentric withdrawal water was withdrawn through a hole in the bottom of the tank. Figure 9 shows experimental paths of floats travelled during fifteen rotations of the tank. Using a fixed camera, the paths were determined by photographing the floats after each complete rotation. The bottom and side wall of the tank were painted black so that the exposures could be made on a single negative.

The experimental pattern of the interior flow is much as predicted by the Ekman model, although the agreement is mainly qualitative in the case of the larger eccentricity. Possibly, the contribution of the potential function Φ_2, which is not considered in figure 8, plays a part here.

5. Concluding remarks

The deformation of the free surface was ignored in the analysis, although a marked drop in water level does occur close to the sink. The velocity distribution near the sink is influenced by this drop in water level during the transient (spin-up) phase of the flow. In the final (quasi-steady) phase, however, the velocities are not affected, since the suction velocity then equals the vertical velocity of the free surface, which does not depend on the ultimate shape the free surface takes on.

Integrating the equation of motion in radial direction, it can be shown that the radius r_1 at which the drop in water level becomes larger than about two per cent of the total depth, is given by

$$r_1 \simeq Q\left(\frac{f}{\nu g h}\right)^{\frac{1}{2}}, \tag{5.1}$$

where g is the gravitational constant. Equation (5.1) in many cases yields fairly small radii r_1. In the case of withdrawal from a constant-density layer in a stratified basin, however, the deformation of the interface may be much larger. The gravitational constant in (5.1) has then to be replaced by $(\Delta\rho/\rho)g$, where $\Delta\rho$ is the density difference between the layers and ρ is the density of the lower layer. $\Delta\rho/\rho$ is a small number in the case of thermal stratification, and the radius r_1 can become considerable.

The research reported here will be continued with experiments on selective withdrawal from a two-layer system, and destratification experiments in which air is locally injected at the bottom of a two-layer system. The major interest in these experiments is in the properties of the interface, such as its stability and frictional behaviour.

REFERENCES

BARCILON, V. 1967 On the motion due to sources and sinks distributed along the vertical boundary of a rotating fluid. *J. Fluid Mech.* **27**, 551–560.

BROWN, S. N. & STEWARTSON, K. 1976 Asymptotic methods in the theory of rotating fluids, in *Asymptotic Methods and Singular Perturbations. Proc. Symp. Appl. Math.* AMS & SIAM.

BURGGRAF, O. R., STEWARTSON, K. & BELCHER, R. J. 1971 Boundary layer induced by a potential vortex. *Phys. Fluids* **14**, 1821–1833.

BURGGRAF, O. R. & FOSTER, M. R. 1977 Continuation or breakdown in tornado-like vortices. *J. Fluid Mech.* **80**, 685–703.

GOOSSENS, L. H. J. & VAN PAGEE, J. A. 1977 Modelling of the near field due to air injection in big reservoirs. *Proc. 17th Cong. IAHR* **1**, 551–560.

GREENSPAN, H. P. 1968 *The Theory of Rotating Fluids.* Cambridge University Press.

HIDE, R. 1968 On source–sink flows in a rotating fluid. *J. Fluid Mech.* **32**, 737–764.

KRANENBURG, C. 1978 On the destratification of lakes and reservoirs using bubble columns. *Delft Univ. Tech.* The Netherlands, *Rep.* no. 78–1.

KUO, H.-H. & VERONIS, G. 1971 The source–sink flow in a rotating system and its oceanic analogy. *J. Fluid Mech.* **45**, 441–464.

LEWELLEN, W. S. 1962 A solution for three-dimensional vortex flows with strong circulation. *J. Fluid Mech.* **14**, 420–432.

NAYFEH, A. H. 1973 *Perturbation Methods.* John Wiley.

TURNER, J. S. 1966 The constraints imposed on tornado-like vortices by the top and bottom boundary conditions. *J. Fluid Mech.* **25**, 377–400.